SOLID-STATE PHYSICS

Twistable electronics with dynamically rotatable heterostructures

Rebeca Ribeiro-Palau[1,2]*†‡, Changjian Zhang[2,3]*, Kenji Watanabe[4], Takashi Taniguchi[4], James Hone[2], Cory R. Dean[1]‡

In heterostructures of two-dimensional materials, electronic properties can vary dramatically with relative interlayer angle. This effect makes it theoretically possible to realize a new class of twistable electronics in which properties can be manipulated on demand by means of rotation. We demonstrate a device architecture in which a layered heterostructure can be dynamically twisted in situ. We study graphene encapsulated by boron nitride, where, at small rotation angles, the device characteristics are dominated by coupling to a long-wavelength moiré superlattice. The ability to investigate arbitrary rotation angle in a single device reveals features of the optical, mechanical, and electronic response in this system not captured in static rotation studies. Our results establish the capability to fabricate twistable electronic devices with dynamically tunable properties.

The weak van der Waals forces between the atomic planes in two-dimensional (2D) materials make it possible to fabricate devices with arbitrary rotational order. Devices could be designed in which electronic properties are controlled by varying the relative twist angle between layers (*1*). Several studies have established that in heterostructures assembled from 2D crystals, electron tunneling between layers varies strongly with rotation (*2*–*8*). In twisted bilayer graphene (two monolayers in direct contact but with an angle mismatch between the layers), several new phenomena have been predicted and observed, including topological valley transport (*9*–*13*) and superconductivity (*14*), as a consequence of angle-dependent interlayer coupling. Likewise, the formation of interlayer excitons in transition metal dichalcogenide heterostructures is highly sensitive to angle (*15*–*17*).

The effect of rotational alignment between conducting and insulating 2D layers can be equally important. An example is provided by graphene coupled to hexagonal boron nitride (BN). The closely matched lattice constants create a large moiré superlattice that develops near zero angle mismatch (*18*, *19*). This superlattice substantially alters the graphene band structure, opening an energy gap at the charge neutrality point (CNP) and creating replica Dirac points at higher energies (*20*–*22*).

Several techniques have been developed to fabricate layered heterostructures with controlled rotation between the layers, including optical alignment of crystal edges (*18*, *20*–*22*), rotational alignment (*23*) during assembly, and self-alignment through thermal annealing (*24*, *25*). However, in each case, an a priori understanding of the crystallographic orientation of each layer is required before assembly; motion between the layers during assembly makes it difficult to achieve precise angle control; and, most importantly, once assembled, the angle cannot be further modified. Here we present an experimental technique that provides on-demand control of the orientation between layers in a van der Waals heterostructure. In a BN/graphene/BN structure, we demonstrate in situ control over the length of the moiré potential and thus achieve dynamic tunability of the optical, mechanical, and electronic properties of the system.

Figure 1A shows a cartoon schematic of our device design. Using the mechanical assembly technique described in (*26*), graphene was placed on top of a large flake of BN, then etched into a Hall bar shape with an oxygen plasma. The graphene layer is intentionally misaligned to this BN, producing a short-wavelength moiré potential that does not substantially alter the intrinsic graphene band structure (*27*). Next, a preshaped BN structure was transferred on top of the graphene. Last, electrical contacts were patterned onto the exposed leads of the graphene (fig. S1). Because of the low mechanical friction between graphene and BN, we could freely rotate and translate this top BN layer by using an atomic force microscope (AFM). Pushing on one of the arms of the uppermost BN structure rotates this layer (Fig. 1, B to D) and changes its crystallographic orientation with respect to the graphene layer. The moiré superlattice wavelength, λ, generated between these crystals is given by

$$\lambda = \frac{(1+\delta)a}{\sqrt{2(1+\delta)[1-\cos(\theta)]+\delta^2}} \quad (1)$$

where $\delta = 0.017$ is the lattice mismatch between graphene and BN, a is the lattice constant of graphene, and θ is the rotational mismatch between the layers. By rotating the top BN layer, the wavelength of the resulting moiré superlattice can be dynamically varied.

Imaging with the same AFM provided a real-time measurement of the orientation of the rotatable BN layer relative to the reference frame of the AFM, which we label as the absolute angle θ_A (for example, Fig. 1, B to D). More important is the relative angle, θ, between the rotatable BN and the encapsulated graphene crystal lattices. To determine this angle, we identified and measured angle-dependent features in the optical Raman spectrum of the heterostructure.

Figure 1F shows a series of Raman spectra measured for θ_A from 34° to 64°. The most striking variation in the Raman spectra was an increase in the full width at half maximum of the 2D peak ($FWHM_{2D}$) (*19*, *28*); a well-defined maximum occurred for this device at ~34.2° (Fig. 1G). On the basis of previous work (*28*), we interpret the peak position as corresponding to zero-angle alignment between the BN and graphene crystals. This peak provides a reference that we could use to determine θ for any orientation of the BN layer.

Our results highlight the robustness of Raman spectroscopy as a tool to characterize the rotational order in these van der Waals heterostructures. Moreover, previous efforts to study effects of twist angle in this system required numerous samples with different fixed angles, whereas here we demonstrate a mapping of the angular dependence with better than 0.2° precision in a single tunable device. One notable disagreement with previous results (*28*) is an overall narrower 2D linewidth in our devices. In previous work, this reduced linewidth was proposed to be a consequence of a reduction of the in-plane strain in fully encapsulated structures, so that areas of full commensuration to the aligned BN disappear (*19*). However, our observation of the same linear trend and a reduced linewidth for the misaligned position, for which no commensurate regions are expected, suggests a different origin. We speculate that this linewidth reduction was caused by the change in the dielectric environment of the graphene caused by the presence of the second BN, as proposed in (*29*). Thus, our results reopen the question of the existence of commensurate states in encapsulated graphene devices. We additionally have identified a shift in the position of the 2D and G peaks with relative angle (fig. S2).

Mechanical resistance while pushing the BN imparted a torque to the AFM tip, causing it to cant away from a vertical position and produce a voltage difference in the AFM's photodetector. This effect can be used to identify variations in frictional forces (Fig. 2A). When sliding the top BN layer with the AFM tip in a translational motion far from alignment, we identified three regimes (Fig. 2B): (i) sliding friction between the tip and the substrate before the tip encountered the BN, (ii) static friction when the tip encountered the BN but resisted translation, and (iii) dynamic friction once the BN began to move.

Figure 2C shows a plot of the change in the tip deflection under continuous rotation (dynamic

[1]Department of Physics, Columbia University, New York, NY, USA. [2]Department of Mechanical Engineering, Columbia University, New York, NY, USA. [3]Department of Electrical Engineering, Columbia University, New York, NY, USA. [4]National Institute for Materials Science, 1-1 Namiki, Tsukuba, Japan.
*These authors contributed equally to this work. †Present address: Centre de Nanosciences et de Nanotechnologies (C2N), CNRS, Université Paris Sud, Université Paris-Saclay, 91120 Palaiseau, France.
‡Corresponding author. Email: rebeca.ribeiro@u-psud.fr (R.R.-P.); cd2478@columbia.edu (C.R.D.)

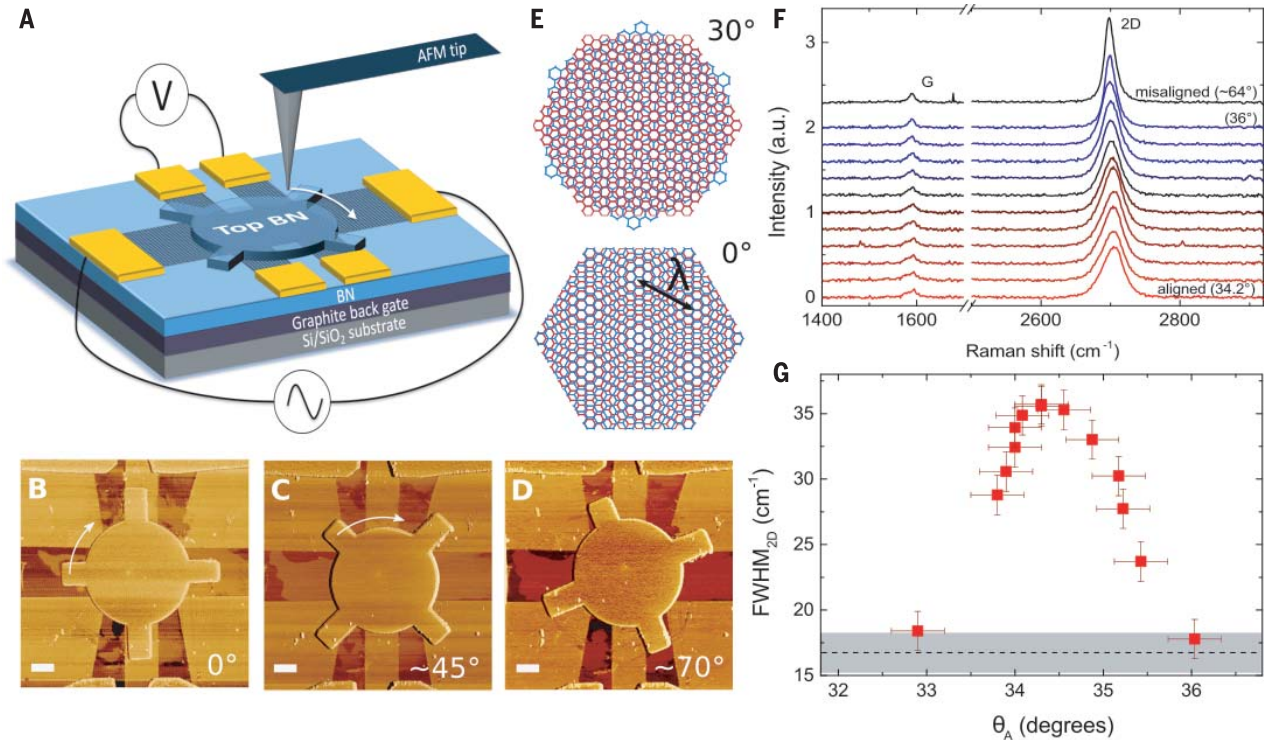

Fig. 1. Rotatable heterostructures. (**A**) Schematic cartoon of the device structure and the experimental technique. BN, hexagonal boron nitride. (**B** to **D**) AFM image of a fabricated device showing three different orientations of the top BN. The angle identified in each panel is the absolute angle referenced to the AFM coordinate system (θ_A). The images were acquired by the same AFM used to rotate the BN layer. Scale bars, 1 μm. (**E**) Schematic illustration of the moiré superlattice arising between graphene (red) and BN (blue) at zero angle. The moiré wavelength, λ, is shown. (**F**) Raman spectrum of the device shown in (B), (C), and (D) for θ_A between 34.2° ± 0.2°and 36.0° ± 0.2°. The black curve shows an additional measurement acquired at ~64°. a.u., arbitrary units. (**G**) FWHM of the 2D peak as a function of the absolute angle. All Raman measurements were taken with the gate bias held at V_g = 0 V. The peak FWHM position identifies zero-angle crystallographic alignment. Error bars represent the precision with which θ can be determined from the AFM topographic images. The dashed line represents the FWHM measured for all angles larger than ~2° away from perfect alignment, with the shaded region representing the associated uncertainty.

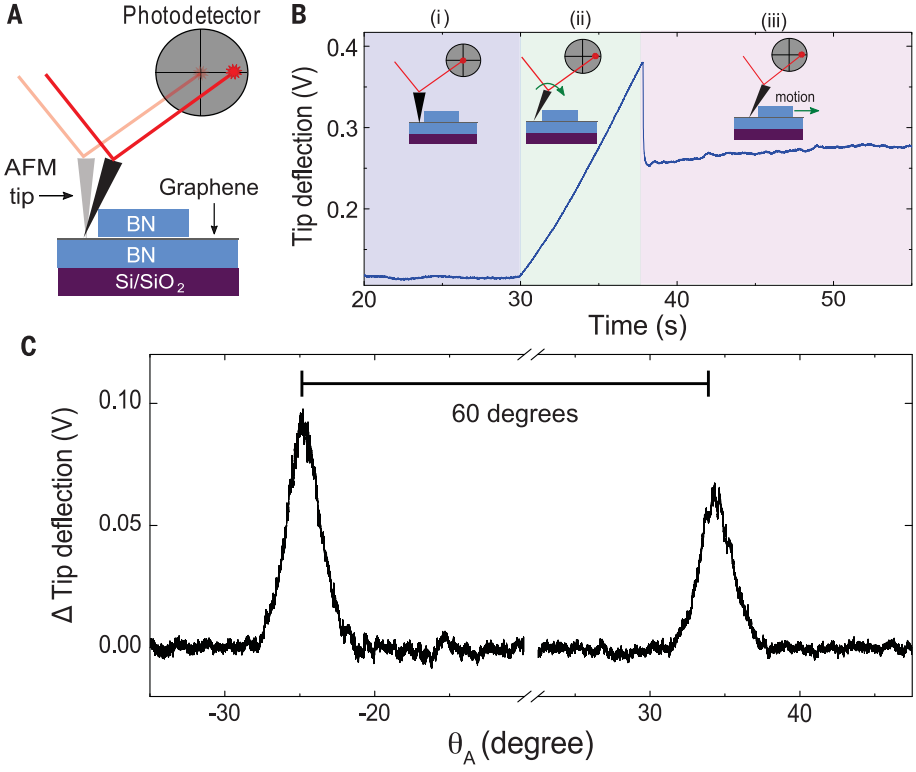

Fig. 2. Mechanical properties. (**A**) Schematic description of friction measurements. When the AFM tip encountered the BN structure, it canted, causing a repositioning of the reflected laser spot in the four-quadrant photodetector. The resulting voltage difference was proportional to the tip cant angle (referred to here as the tip deflection) and served as a measure of the torque force acting at the end of the tip. (**B**) Tip deflection versus time in a translational push of the upper BN structure. Different regimes of the measurement were identified: (i) As the tip dragged along the surface, tip-substrate friction resulted in a steady-state tip deflection. (ii) When the tip encountered the BN structure, it initially resisted translation, and the tip deflection increased. We refer to this as the static friction regime. (iii) Once the BN was in motion, the tip deflection relaxed slightly, providing a measure of the dynamic friction at the BN-graphene interface. (**C**) Tip deflection versus absolute angle, measured during a continuous rotation of the BN. Two peaks were observed, spaced 60° apart.

friction), in which we subtracted the background caused by piezoelectric drift and residual friction. Two prominent peaks are separated by 60°. This result closely resembles a previous measurement of friction between two graphitic structures in which a transition from superlubricity (where the structures are in an incommensurate position and the atomic shear forces are negligible) to a dissipative state was observed at commensurate angles of the threefold symmetric hexagonal lattices (*30*–*32*). However, because of the lattice mismatch between graphene and BN, there is not true lattice commensurability at any angle, and the increase in the friction should have a different origin. Recent numerical simulations suggest that contributions of the moiré superlattice to the frictional force cannot be neglected and are expected to be maximal for aligned layers (*33*), which could explain our experimental result. Our device structure allows us to study mechanical properties, such as frictional force, in atomically flat materials without rugosity contributions. These results also highlight the possibility of using the friction response as an in situ method to monitor and control layer alignment in heterostructures.

Our device design enabled us to measure electron transport in the active layer (in this case, graphene) while changing the relative orientation of the overlayer. Figure 3A shows a plot of the four-terminal resistance of the graphene layer as a function of back gate voltage V_g for different values of θ at room temperature. Near θ = 0, additional satellite resistance peaks appear symmetrically in density around the CNP. This result is consistent with the emergence of satellite Dirac points induced by scattering from the moiré superlattice potential (*18*, *20*–*22*).

As θ increased from zero, the satellite peaks diminished in intensity and moved further from the CNP to higher gate values. To analyze this behavior more quantitatively, Fig. 3B plots the satellite peak position in V_g versus θ determined from the AFM imaging. The measured position shows excellent agreement with the values of carrier density n at which the full filling of the miniband occurs, $n = 8/\sqrt{3\lambda^2}$, where the carrier density and gate voltage are related by $n = C_g(V_g - V_{CNP})$, C_g is the capacitive coupling of the electrostatic gate, and λ is given by Eq. 1 (*18*, *20*–*22*). The error bars in Fig. 3B, ~±0.2°, reflect the precision with which θ can be determined from the AFM topographic images. Determining θ from the V_g position of the satellite peak at low temperature provides a more accurate measurement with uncertainty less than ±0.1°. However, this method of determining the angle is limited to only a few degrees where the satellite peak remains within an accessible density range.

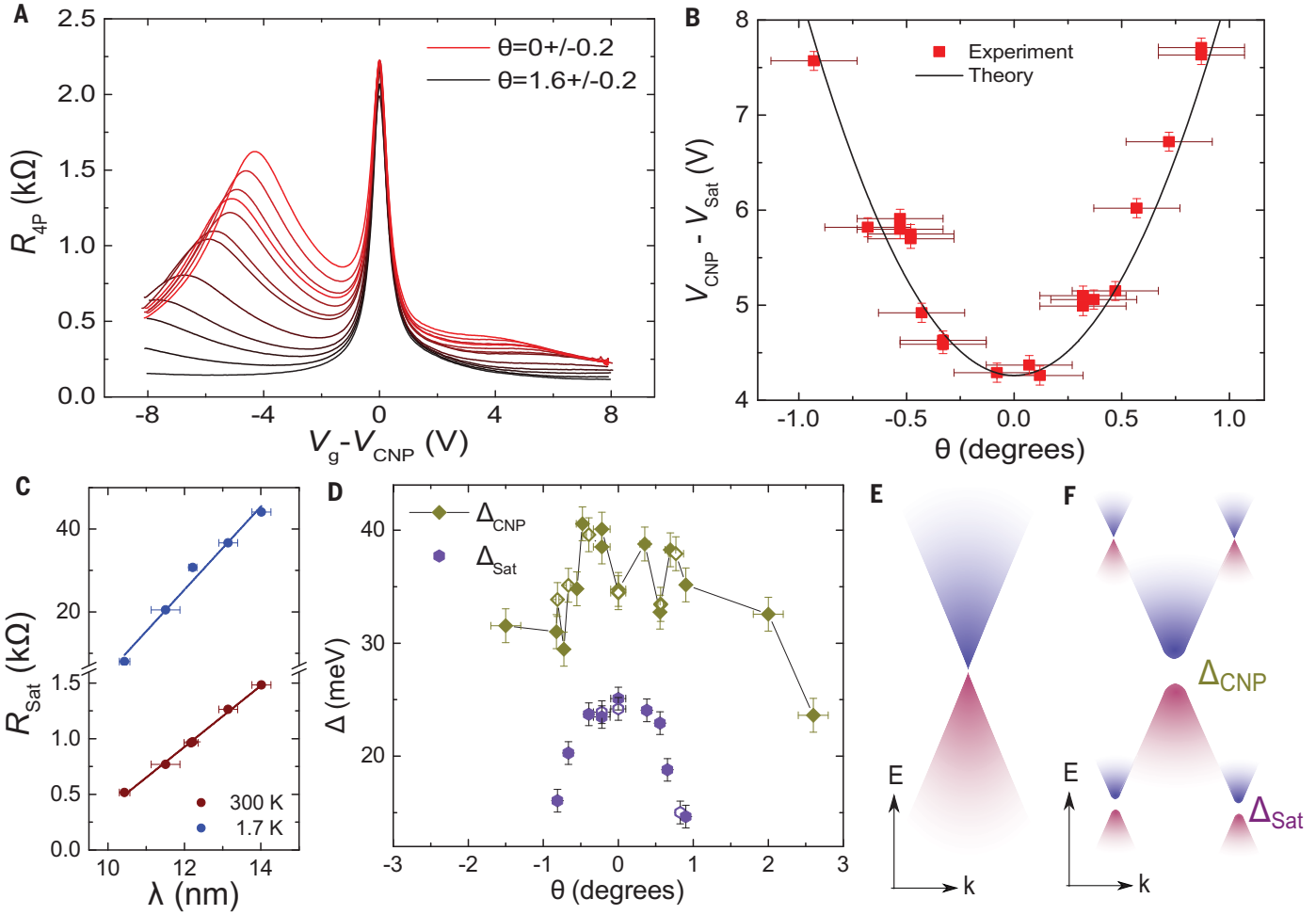

Fig. 3. Electronic transport properties. (**A**) Four-terminal resistance (R_{4P}) as a function of V_g for different alignments of the graphene/BN structure, acquired at room temperature. (**B**) Position of the satellite peak in gate voltage as a function of the relative angle. The ±0.2° error in the angle reports the precision achieved with the AFM imaging in tapping mode. The vertical error bars represent the maximum uncertainty with which we can determine the position of the satellite peak owing to the broadening of the peak. (**C**) Linear dependence of the maximum value of the four-terminal resistance at the satellite peak at 300 K (red) and 1.7 K (blue) as a function of the moiré length. (**D**) Energy gap, measured by thermal activation, for the satellite peak (circles) and the charge neutrality point (diamonds) as a function of the relative angle. Open symbols represent a repeated measurement at a given angle after moving through other angles and thermally cycling. (**E**) Schematic band structure for native graphene and (**F**) for a graphene-BN heterostructure with a small twist angle. *E*, energy; *k*, momentum.

Plotting the resistance of the satellite peak versus λ for a single device revealed an apparently linear variation in the magnitude of the satellite peak resistance (Fig. 3C). The resistance of the CNP did not change linearly with θ in this range (fig. S3). The origin of this linear dependence is not known. This striking observation highlights how a physical phenomenon previously obscured (*18*, *20*–*22*) by sample-to-sample variations became clear by varying rotation in a single sample.

We measured the energy gap versus angle at both the central and satellite Dirac points by thermal activation. The gap magnitudes (Fig. 3D) were in good agreement with electronic transport measurements in encapsulated (*34*) and nonencapsulated devices (*19*, *20*), optical measurements made in epitaxial BN/graphene structures (*35*), and theoretical calculations (*36*). The energy gap of the satellite peak decreased smoothly away from θ = 0. In contrast, the energy gap at the CNP displayed a more complex behavior near θ = 0 and only decreased appreciably for $|\theta| > 2°$.

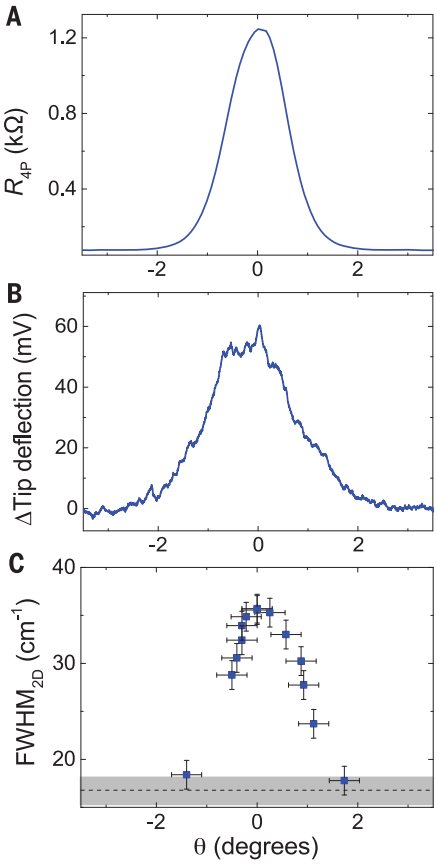

Fig. 4. Compilation of observations with the angle control technique. (**A**) Four-terminal resistance as a function of the relative angle measured at a carrier density of -1.9×10^{12} cm^{-1}. (**B**) Tip deflection in friction measured simultaneously with the electronic transport. (**C**) FWHM of the 2D peak of the Raman spectrum as a function of the relative angle. All measurements were performed in the same device.

The origin of the extra structure observed for the CNP remains to be understood. However, this result does not appear to be simple experimental noise because several gap values were confirmed to be reproducible when measured nonconsecutively (i.e., after thermally cycling and rotating through different angles and back). The difference in behavior of the two energy gaps, which would be impossible to observe in a study that used multiple samples at fixed angles (*34*), reflects their different physical origins and highlights the importance of these results in fully understanding the band structure modifications resulting from variations in angular alignment (Fig. 3, E and F). The persistence of an energy gap at the CNP in encapsulated devices for angles beyond that at which a commensurate-incommensurate transition was previously identified (*19*) suggests that this energy gap is not related solely to the presence of a commensurate state.

Figure 4 shows a direct comparison of the optical, mechanical, and electronic response versus angle measured in the same device. The four-probe resistance (Fig. 4A), the maximum tip deflection signal (friction; Fig. 4B), and the maximum FWHM of the Raman 2D peak (Fig. 4C) coincide exactly, confirming the relation between these properties. The four-probe resistance (Fig. 4A) and friction response (Fig. 4B) were acquired simultaneously at a fixed carrier density of 1.9×10^{12} cm^{-1} (corresponding to the dashed line in fig. S4) while continuously rotating the BN layer. At this relatively high carrier density, the bulk resistance was modulated by more than an order of magnitude over <2° of rotation (at cryogenic temperatures, this modulation increases to more than two orders of magnitude; supplementary materials).

Our demonstration of rotatable heterostructures with dynamically tunable device characteristics presents an opportunity in device engineering. Although we investigated BN-encapsulated graphene as a model tunable system, this technique is readily extendable to generic heterostructures fabricated from 2D materials. In addition to band structure tunability, emergent phases such as superconductivity and magnetism may be controllably varied with rotation.

REFERENCES AND NOTES

1. S. Carr *et al.*, *Phys. Rev. B* **95**, 075420 (2017).
2. L. Britnell *et al.*, *Nat. Commun.* **4**, 1794 (2013).
3. A. Mishchenko *et al.*, *Nat. Nanotechnol.* **9**, 808–813 (2014).
4. M. T. Greenaway *et al.*, *Nat. Phys.* **11**, 1057–1062 (2015).
5. B. Fallahazad *et al.*, *Nano Lett.* **15**, 428–433 (2015).
6. T. Chari, R. Ribeiro-Palau, C. R. Dean, K. Shepard, *Nano Lett.* **16**, 4477–4482 (2016).
7. E. Koren *et al.*, *Nat. Nanotechnol.* **11**, 752–757 (2016).
8. J. R. Wallbank *et al.*, *Science* **353**, 575–579 (2016).
9. L. A. Gonzalez-Arraga, J. L. Lado, F. Guinea, P. San-Jose, *Phys. Rev. Lett.* **119**, 107201 (2017).
10. Y. Cao *et al.*, *Phys. Rev. Lett.* **117**, 116804 (2016).
11. J. D. Sanchez-Yamagishi *et al.*, *Nat. Nanotechnol.* **12**, 118–122 (2017).
12. L. Ju *et al.*, *Nature* **520**, 650–655 (2015).
13. C.-J. Kim *et al.*, *Nat. Nanotechnol.* **11**, 520–524 (2016).
14. Y. Cao *et al.*, *Nature* **556**, 43–50 (2018).
15. H. Yu, Y. Wang, Q. Tong, X. Xu, W. Yao, *Phys. Rev. Lett.* **115**, 187002 (2015).
16. P. Rivera *et al.*, *Science* **351**, 688–691 (2016).
17. P. Rivera *et al.*, *Nat. Commun.* **6**, 6242 (2015).
18. M. Yankowitz *et al.*, *Nat. Phys.* **8**, 382–386 (2012).
19. C. R. Woods *et al.*, *Nat. Phys.* **10**, 451–456 (2014).
20. B. Hunt *et al.*, *Science* **340**, 1427–1430 (2013).
21. L. A. Ponomarenko *et al.*, *Nature* **497**, 594–597 (2013).
22. C. R. Dean *et al.*, *Nature* **497**, 598–602 (2013).
23. K. Kim *et al.*, *Nano Lett.* **16**, 1989–1995 (2016).
24. D. Wang *et al.*, *Phys. Rev. Lett.* **116**, 126101 (2016).
25. C. R. Woods *et al.*, *Nat. Commun.* **7**, 10800 (2016).
26. L. Wang *et al.*, *Science* **342**, 614–617 (2013).
27. C. R. Dean *et al.*, *Nat. Nanotechnol.* **5**, 722–726 (2010).
28. A. Eckmann *et al.*, *Nano Lett.* **13**, 5242–5246 (2013).
29. C. Neumann *et al.*, *Nat. Commun.* **6**, 8429 (2015).
30. M. Dienwiebel *et al.*, *Phys. Rev. Lett.* **92**, 126101 (2004).
31. Z. Liu *et al.*, *Phys. Rev. Lett.* **108**, 205503 (2012).
32. A. E. Filippov, M. Dienwiebel, J. W. M. Frenken, J. Klafter, M. Urbakh, *Phys. Rev. Lett.* **100**, 046102 (2008).
33. E. Koren, U. Duerig, *Phys. Rev. B* **94**, 045401 (2016).
34. L. Wang *et al.*, *Science* **350**, 1231–1234 (2015).
35. Z.-G. Chen *et al.*, *Nat. Commun.* **5**, 4461 (2014).
36. J. C. W. Song, A. V. Shytov, L. S. Levitov, *Phys. Rev. Lett.* **111**, 266801 (2013).

ACKNOWLEDGMENTS

We acknowledge discussions with M. Yankowitz and A. Botello-Mendez, and we acknowledge J. Huerta, N. Finney, T. Chari, S. Chen, and M. Gustafsson for technical support. **Funding:** This research was supported by the NSF MRSEC program through Columbia University's Center for Precision Assembly of Superstratic and Superatomic Solids (DMR-1420634). C.R.D. acknowledges partial support by the National Science Foundation (DMR-1462383). **Author contributions:** R.R.-P. and C.R.D. designed the experiment. R.R.-P. and C.Z. fabricated the samples, performed the experiments, analyzed the data, and wrote the paper. T.T. and K.W. grew the crystals of hexagonal boron nitride. J.H. and C.R.D. advised on experiments, data analysis, and writing the paper. **Competing interests:** None declared. **Data and materials availability:** All data needed to evaluate the conclusions are present in the paper or the supplementary materials.

SUPPLEMENTARY MATERIALS

www.sciencemag.org/content/361/6403/690/suppl/DC1
Materials and Methods
Figs. S1 to S9
References (*37*, *38*)

6 April 2018; accepted 11 June 2018
10.1126/science.aat6981

Science

Twistable electronics with dynamically rotatable heterostructures

Rebeca Ribeiro-PalauChangjian ZhangKenji WatanabeTakashi TaniguchiJames HoneCory R. Dean

Science, 361 (6403), • DOI: 10.1126/science.aat6981

Controlling two-dimensional twist

In heterostructures assembled from two-dimensional materials such as graphene, electron tunneling between layers varies strongly with the rotation angle between the crystal lattices. Usually, the twist angle between layers is fixed after assembly. Ribeiro-Palau *et al.* encapsulated graphene with boron nitride, but the top boron nitride flake was shaped so that an atomic force microscope tip could push on it to vary the twist angle by as little as 0.2°. They observed variations with twist angle in properties such as the charge neutrality point, which would be difficult to observe in static rotated structures.

Science, this issue p. 690

Science (ISSN 1095-9203) is published by the American Association for the Advancement of Science. 1200 New York Avenue NW, Washington, DC 20005. The title *Science* is a registered trademark of AAAS.